AIMS Materials Science, 8(6): 881–898.
DOI: 10.3934/matersci.2021054
Received: 25 October 2021
Accepted: 09 December 2021
Published: 14 December 2021

http://www.aimspress.com/journal/Materials

Research article

Development of compressive testing device for glass fiber based single face corrugated structure sheet, and estimation of buckling strength of straight panel of that structure sheet

Songtam Laosuwan[1,2] and Shigeru Nagasawa[1,*]

[1] Department of Mechanical Engineering, Nagaoka University of Technology, 1603-1 Kamitomioka, Nagaoka, Niigata 940-2188, Japan
[2] Department of Mechanical Engineering, Pathumwan Institute of Technology, 833 Rama 1 Rd., Pathumwan, Bangkok, 10330 Thailand

* **Correspondence**: Email: snaga@mech.nagaokaut.ac.jp.

Abstract: This work aims to reveal the in-plane-compressive characteristics of Glass Fibre based single face corrugated Structure Sheet (GFSS) by developing a loading holder of the both ends of the panel of GFSS in the direction of the cross machine direction. A grooved end-support device was developed and exmined. In order to set stably and quickly a straight panel of GFSS on the compressive-testing apparatus, the width and the depth of the holder's groove were varied against the geometrical size of the panel, and the stability and reproducibility of compressive deformation of the panel was experimentally investigated. When changing the height of the panel and reinforcing the both ends of the panel by dipping instant adhesives, the deformation behavior and the buckling strength was characterized in three modes: a short height crushing without lateral deflection, a small lateral deflection mode as the intermediate state, and a triangle-like folding as a long height crushing.

Keywords: end crush; bending; buckling; fabrics of glass fibre; compressive strength

Abbreviations: λ: A wave length (pitch) of GFSS, 7.1 mm; h_o: t_L; t_W: A height of GFSS, a thickness of liner, and a thickness of wave layer; h_f: A height of free zone of panel supported by upper/lower grooves on holder; h_g: A depth of groove of the edge holder, 10 mm; w_{gs}: A width of groove of the edge holder for the straight panel, 3, 3.2, 3.5 and 4.0 mm; H: A height of specimen of GFSS, $H = 2h_g + h_f$; B_S: A width of straight specimen of GFSS, 46 mm (=6.5 λ). It includes closed 6 waves; F: A

compressive force on a GFSS panel in the heightwise direction (N), $f = F/B$: a compressive line force applied to GFSS (N/mm). The width of panel was chosen as B_S; f_p: A peak maximum line force of $f = F/B$ during a compressive test; d: A compressive displacement of the fixture on a press machine at the heightwise compressive test of GFSS; d_p: A corresponded displacement of the fixture to the peak maximum line force f_p; $F_{cr} = \pi^2 EI/(kh_f)^2$: An Eulerian critical buckling force at a compressive test of straight panel. Here, k was 0.5 when the upper/lower ends of panel were fixed with rotation. I is the equivalent second moment of area in the in-plane cross (heigtwise) direction of GFSS when $B = B_S$, while E is the equivalent Young's modulus of GFSS. $f_{cr} = F_{cr}/B_S$ is the critical buckling strength as line force (N/mm); $EI = (B_S/B_{3p})(L^3/48)(\Delta F/\Delta\delta)$: A bending stiffness in the in-plane cross (heigtwise) direction of GFSS panel when $B = B$s. Here, L = 30 mm was a span length of specimen, B_{3p} = 25 mm = 3.5λ was a width of specimen at three-point-bending test. The gradient of force by deflection $\Delta F/\Delta\delta$ was experimentally measured from a three point bending test of GFSS

1. Introduction

Glass fiber based structure sheet (GFSS) is commercially produced and used as a core sheet for making a reinforced plastics structure [1]. A combination of two layers as the liner and the corrugated medium is called as a single face type in the packaging industry of corrugated fiberboard (CFB) [2–4]. A GFSS is geometrically similar to the single face structure of CFB, but the joint mechanism of liner and wave layer is different from that of CFB. They (a liner and a wave layer) are interweaved against common crossed fibres of liner layer. A GFSS is composed of the wave and the liner layers, which are periodically intersected with each other. The wave layer makes a bridge across the liner layer by knitting. As for the mechanical properties of CFBs, there are various testing and measurement methods such as the standard JIS Z 0401, JIS Z 0212. To know the mechanical strength of CFBs, the flat crush test (out-of-plane compressive test), the edgewise crush test (end crush test, an in-plane height wise compressive test) [5–8], the ring crush test (in-plane compressive test) of a liner or intermediate sheet, and a compression test on a corrugated box are well known. However, since a GFSS is based on glass fibre fabrics, it is seemed that these testing methods are not applied to estimate the mechanical properties of GFSS without any consideration or modification.

GFSS is made of single-face corrugated glass fiber fabrics and a light-weight sheet. It has a high stiffness in the in-plane height wise and flexural for bending in the out-of-plane. GFSS seems to be suitable for making a curved structure of reinforced resin. It is convenient for making electric wave shielding and then well used for making a rotor of electric driving motor. The authors developed a flexible-fitted fixture for gripping the specimen and investigated the tensile strength and the elongated behavior of GFSS in the producing machine direction (Machine direction, MD) [9,10]. Regarding the in-plane tensile test of GFSS in the MD, an advanced fixing condition of GFSS specimen was developed using a combination of insert pins and instant adhesives. This fixture device was designed by referring the tensile test method of CFB using fixing pin and wax filling [11]. Wahab et al. [12] studied a fundamental usage of single parallel pins for fixing a double face corrugated fiberboard (CFB) made of kraft paper. Cox [13] has studied effects of orientation of the fibers on the stiffness and the strength of paper and other fibrous materials.

When designing various packaging panels of GFSS, the in-plane height wise compressive (or buckling) strength of GFSS is necessary for estimating the mechanical behavior of panel structure, and needless to say, that of a resin-reinforced GFSS is important for determining the strength of

structural panels. But the in-plane height wise compressive strength of GFSS is not sufficiently investigated due to the fragile behavior [2] and the complexity of three-dimensional structure composed of a wave layer and a liner layer [5].

As advantages, GFSS has easiness of cylindrical bending for making a curved wall structure. However, the mechanical properties of GFSS under bent condition was not well known due to its complex structure and fragile property. The buckling mode of breaking zone of cylinderical wall is not well understand yet.

Therefore, in this work, to reveal the compressive strength of a straight panel of GFSS, a fixing device for compressive loading on a vertical (height wise) panel of GFSS was developed, and the compressive test of the straight panel was carried out, when varying the groove profile of the fixture for supporting the upper/lower ends of GFSS panel.

2. Materials and methods

2.1. Principle of in-plane compressive test and condition of specimen

The primary specifications of GFSS are the basic weight or the average density of glass wires, the pitch size of the flute and so on. A prepared specimen of GFSS was illustrated in Figure 1 [1]. Here, a total outside height of h_0, a wave length of λ, a liner thickness of t_w, a wave layer thickness of t_L of GFSS were arranged in Table 1. According to JIS Z0104-1003, since B type flute of corrugated paper board has h_o = 3 mm, λ = 6 mm, the specification of GFSS is geometrically similar to the B type flute. Raw sheets of GFSS were produced using the twisted yard, E-glass of Nittobo, ECG75-1/2-3.8S (Fineness: 135 (fineness: 135 ± 8.1 TEX, a diameter of filament: 9.5 μm, number of twists: 3.8 per 25 mm) [14–16]. After knitting, a few of acrylic based adhesives were injected on the raw sheets of GFSS. The cord count (density) of the upper wave layer and the lower liner of GFSS was 25 ± 1 per 25mm width in the longitudinal direction (Machine transforming direction) and in the lateral direction (cross machine direction), respectively.

As an advanced purpose, a compressive strength of box structure of GFSS is attractive. Figure 2a illustrates a box of GFSS subjected to a compressive load. However, since GFSS is a complex structural sheet, an in-plane heightwise compressive strength of a simple straight panel of GFSS is here investigated, as shown in Figure 2b.

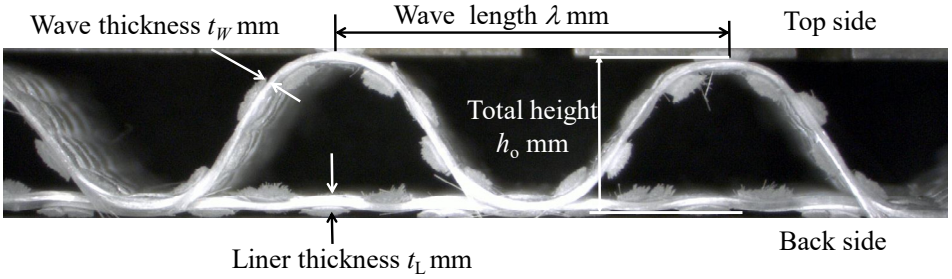

Figure 1. Side view of two flutes of GFSS (glass fibre based single face corrugated structure sheet).

Table 1. Structural dimensions of a side view of GFSS.

Geometrical parameters of GFSS shown in Figure 3	Average of 5 samples (maximum-minimum)
Total outside height, h_o (mm)	3.0 (3.05–2.95)
Wave-length λ (mm)	7.1 (6.86–7.58)
Liner thickness t_L (mm)	0.25 (0.17–0.31)
Wave thickness t_W (mm)	0.25 (0.14–0.30)

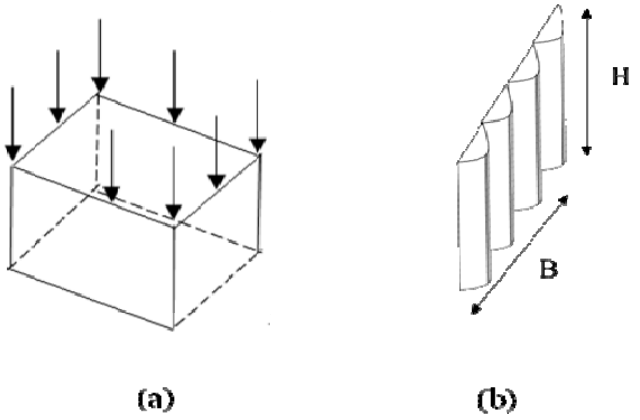

Figure 2. General views of a straight panel of GFSS in heightwise direction and box structure as example of closed panels subjected to in-plane heightwise load. (a) Compression of a box or closed panels, (b) General view of a rectangle straight panel of GFSS.

When considering the compressive strength of such a panel which is some elemental parts of a box, a central zone of panel is often noted from the aspects of panel strength. The height of panel is restricted by a kind of folded hinge of top or bottom flap. The upper/lower edges of panel are normally fixed to prohibit to rotate in the out-of-plane of panel. Therefore, when varying the height of panel in the heightwise direction, the deformation of panel seems to be classified in two modes, shown in Figure 3a,b. The former ($H \leq 4h_0$) is understood as an edgewise crush (ISO 3037, edge crush test, ECT) without any lateral deflection of panel. Here, regarding the B flute type, a height of panel specimen is 32 mm for ECT, whereas the height of guide block is chosen as 20 mm [7,8]. Therefore, a free height of panel is expected 12 mm as 4 times of h_o. The latter ($H >> 4h_0$) seems to be deflected in the lateral direction at the central zone, while the upper/lower edges are fixed with rotation in the out-of-plane. Since the deflected direction of out-of-plane is generally unknown, the deflection was tentatively assumed to be on a wave layer side (b-1) or a liner layer side (b-2) in this picture.

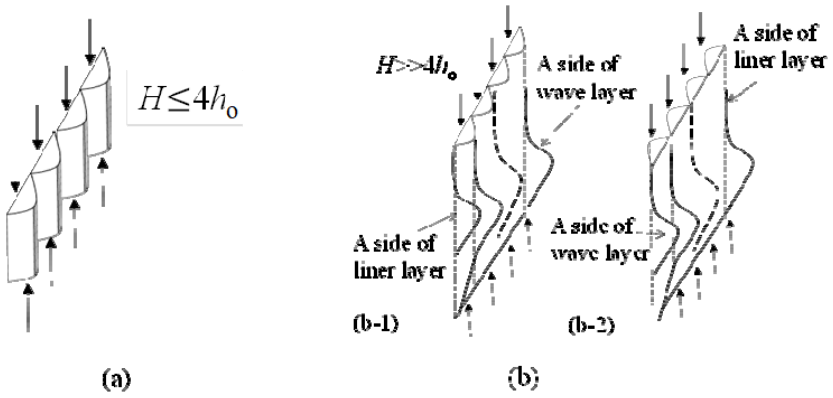

Figure 3. Deflection modes of GFSS panel subjected to heightwise compressive load when fixing out-of-plane rotational freedom of upper/lower edges of panel. (a) Compressive state of a short height panel at the end crush testing without lateral bending; (b) Compressive state of a long height panel at the lateral buckling of tall pillar or shell.

2.2. Experimental conditions of straight panel at compressive loading

2.2.1. Set-up condition of straight panel specimen

To investigate the heightwise buckling strength of GFSS, a grooved aluminum plate (edge holder) was prepared as shown in Figure 4a, which was used for compressing a straight panel of GFSS. Figure 4b illustrated an assembled state of a straight panel of GFSS using the upper/lower edge holders. The upper edge holder was set up on the upper rod of the compressive machine, while the lower edge holder was mounted on the base block of the compressive machine. The straight panel of GFSS was inserted into the upper and lower grooves without applying any self weight of the upper holder to the panel. For examining the compressive test of a 46 mm-width panel of GFSS, the maximum capacity of the load cell was 10 kN.

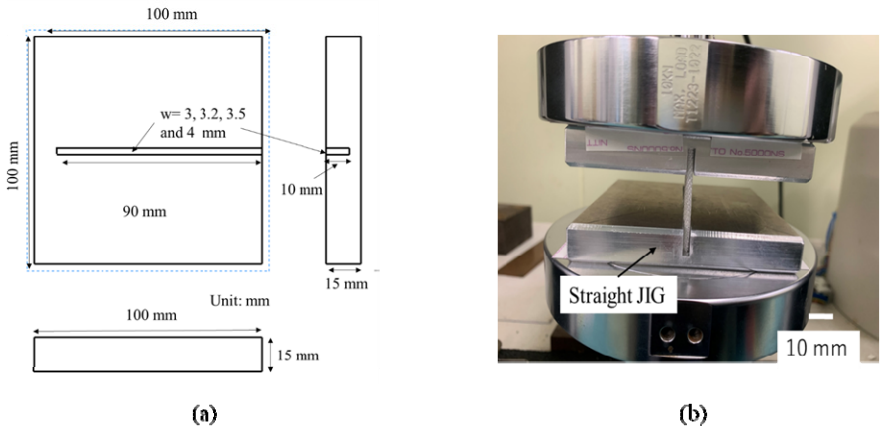

Figure 4. Experimental apparatus of in-plane compressive test of a straight panel of GFSS. (a) A half of edge holder of straight panel of GFSS, (b) Setup of straight panel on upper/lower edge holders.

The depth of groove h_g was chosen as 10 mm which was deeper than 3 times of the height of GFSS h_o = 3.0 mm. When using the zero depth of groove as the panel holder, the panel of GFSS could not be kept in the vertical attitude. Therefore, appropriate groove is necessary for the compressive test. The width of groove w_{gS} was chosen as 3.0, 3.2, 3.5 and 4.0 mm, which were compared for knowing the effects of the clearance w_{gS}-h_o. Herein, w_{gS} = 3.0 mm was assumed to be the respresentative width when chaning the free height of panel.

Figure 5 shows a zoomed-up side view of GFSS specimen and a schematic of specimen which was clamped by the upper/lower edge holders to know the size effects of the free zone. The number of specimens were five for each case. The side views of compressed GFSS was recorded as video movies for knowing occurred deflection modes. As for the size of specimen of GFSS in the case of straight panel, the width of specimen B_S = 46 mm was fixed as 6.5 λ of the wave layer, while the height of specimen H = 25, 30, 40, 50, 60, 70, 80, 90, 100, 110, 120, 130 and 140 mm was chosen. Namely, the height of free zone of specimen $h_f = H\text{-}2h_g$ = 5–120 mm was chosen. The compressive displacement of the edge holder was chosen as d = 4 mm at h_f = 5 mm, and d = 8 mm for h_f = 10–120 mm, while the compressive velocity V = 0.21 mm/s was fixed during the compressive test. Through the compressive test of the straight panel of GFSS, the relationship between the displacement d and the line force $f = F/B_S$ was measured and the peak maximum line force f_p was investigated.

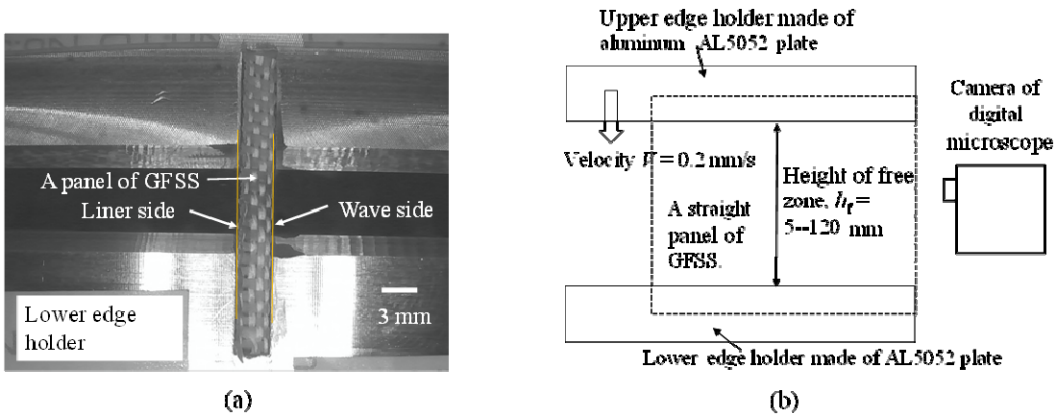

Figure 5. Zoomed-up views of a straight panel of GFSS for compressive test. (a) Side view of compressed panel; (b) Straight panel and upper/lower holders.

Since the crush of both ends of a panel affects the initial buckling behavior of the panel, a brief reinforcement by adding instant adhesives on the both ends of the panel was considered as shown in Figure 6. On four points on the edge of 6 waves of a straight panel, instant adhesives (liquid arone alpha) were dipped, and the panel was dried for 24 h after dipping. Comparing a weight variation of the panel with this dipping, its additional weight was totally 0.116 g (as the average) on the edge of the straight panel.

All the experiments were carried out in a room temperature of 296 K and in a humidity of 50% RH. Five pieces of GFSS specimen were examined for the basic and reinforced models.

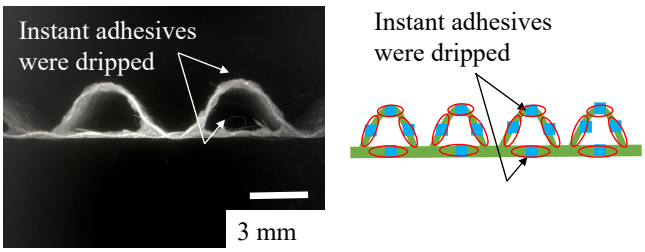

Figure 6. Some brief reinforcement of edges of GFSS by dipping instant adhesives at a straight panel.

2.2.2. Discussion model of critical buckling strength on a straight panel

Regarding the out-of-plane bending stiffness of GFSS, the three point bending test [17] was applied to a rectangle sheet of GFSS which had a width of B_{3p} = 25 mm and a heightwise length of 35 mm. The punching tool had a round-edge of 0.36 mm radius and the supporting anvil had a groove which had a span length of L = 30 mm. Since the GFSS was asymmetric sturucture of wave layer and liner layer, as two kinds of pushing direction, the liner side and the wave side were pushed respectively by the punching tool, while the GFSS was mounted on the supporting anvil. From the Timosienko's beam deflection theory [17], the bending stiffness of $D = EI$ is estimated from Eq 1. Here, the gradient of force by deflection $\Delta F/\Delta\delta$ was experimentally estimated as the first order coefficient of linear approximation for the early stage of 0.03 mm < δ < 0.4 mm (corresponding from 20% to 80% of peak maximum load) from the three point bendind test of GFSS.

$$D{=}EI = (B_S/B_{3p})(L^3/48)(\Delta F/\Delta\delta) \quad (1)$$

To estimate the critical buckling strength of a straight panel supported by the upper/lower grooves, a simple beam buckling theory by Timosienko was tried to be applied to this compressing test. Denoting the free surface length of panel as h_f, the out-of-plane bending stiffness as $D = EI$ (E: Equivalent Young modulus, I: the second order sectional moment of 7.5 wave length = B_S), and the factor of boundary condition as k, a line force of critical buckling force f_{CR} is expressed as Eq 2 [18].

$$F_{CR}/B_S = f_{CR} = \pi^2 D/B_S/(kh_f)^2 \quad (2)$$

Herein, since the both (upper/lower) ends of a panel were assumed to be fixed with rotation, k was determined as 0.5. From the three point bending flexural test of GFSS across the flute structure, as a value of D was analyzed and gotten from Eq 1, the critical line force f_{CR} was estimated by Eq 2.

3. Results and discussions

3.1. Mechanical sizes and properties of GFSS

Seeing the 3 points bending flexural test of GFSS specimens (shown in Figure 7), values of the bending stiffness D (=EI) (estimated by Eq 2), the sectional area A, and the second moment of area I calculated from a CAD data were shown in Table 2. It was found that the out-of-plane bending stiffness of GFSS was a little different with respect to the pushing direction. Namely, the bending stiffness of wave layer's pushing was about 32% larger than that of liner layer's pushing.

Referring the tensile test of GFSS [10], a nominal tensile Young's modulus of a plain glass fibre sheet which was equivalent to the liner sheet of GFSS was estimated as E = 6.2–6.3 GPa. Therefore, the three-point-bending test based Young's moudulus was about 18% compared with the in-plain tensile mode.

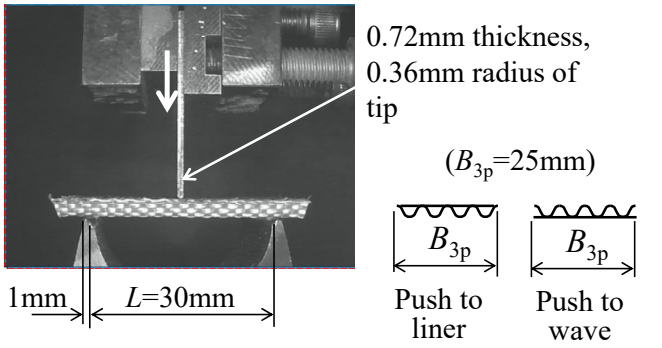

(a) Front view of specimen (b) Side view of specimen

Figure 7 Schematics of three point bending test of GFSS specimen.

Table 2. In-plane mechanical sizes and properties of GFSS which had 6.5 waves of flutes.

Mechanical condition of specimen and fixture	Estimated Young's modulus E MPa from the measured EI by the calculated I.	Measured bending stiffness D (=EI) (Yong's modulus x a second moment of area) when L = 30 mm	Sectional area of 6.5 waves of GFSS A (mm^2), calculated from a CAD drawing data	Second moment of area of 6.5 waves of GFSS, I (mm^4), calculated from a CAD drawing data
The three-point bending test of GFSS (liner layer was pressed by using a blade).	21609/21.66 = 997.6 MPa	21609 Nmm^2 (Standard deviation, 403.4 Nmm^2, 1.8%)	26.52 mm^2	21.66 mm^4
The three-point bending test of GFSS (wave layer was pressed by using a blade).	28595/21.66 = 1320.2 MPa	28595 Nmm^2 (Standard deviation, 876.0 Nmm^2, 3.1%)		

3.2. Buckling behavior of straight panel and load response

Figure 8 shows representative compression processes of straight panel which had h_f = 5, 20, 40 and 80 mm at w_{gs} = 3mm without dipping instant adhesives. In Figure 8a h_f = 5 mm and (b) h_f = 20 mm for the displacement of 5 mm, there were not any large lateral deflection (in the out-of-plane), but a local bulging appeared to occur in the in-plane direction at the free zone and also at the both ends of the panel. Figure 8c shows a representative compression process of a middle span of h_f = 40 mm, while (d) shows that of a long span of h_f = 80 mm. When h_f > 30mm, the triangular buckling as a lateral deflection occurred at the middle zone. Herein, the moving direction of deflection was observed in two directions with the liner side and the wave side of the panel.

Regarding the compressive test of the straight panel without dipping instant adhesions, Figure 9 shows the relationship between the compressive force $f = F/B_S$ per unit width of the specimen (the line force) and the displacement of upper edge holder d. The line force f was kept in a certain resistance in a range of d < 8 mm at h_f < 30 mm, while it had a peak maximum of line force in a range of d < 3 mm at h_f > 30 mm. Seeing Figures 8 and 9, since the critical condition of lateral

deflection as the out-of-plane buckling appeared to occur at h_f = 30 mm, it was found that the peak maximum line force (at the early stage for d < 3 mm) corresponded to the occurrence of out-of-plane buckling. Referring the crtical condition of edge crush test (ECT), the corresponded height of free zone is estimated as $h_f = 4h_0$ = 12 mm. In this experiment without dipping instant adhesives, since the both ends of the panel was easily crushed due to its fragile structure and then as the in-plane reaction force decreased, the experimental critical condition of lateral buckling appeared to increase up to h_f = 30 mm.

Figure 10 shows representative compression processes of a straight panel which had h_f = 5, 20, 40, 80 mm and w_{gs} = 3 mm when dipping instant adhesives on the both ends. Namely, in this case, the both ends of the panel were reinforced by a small volume of resin materials.

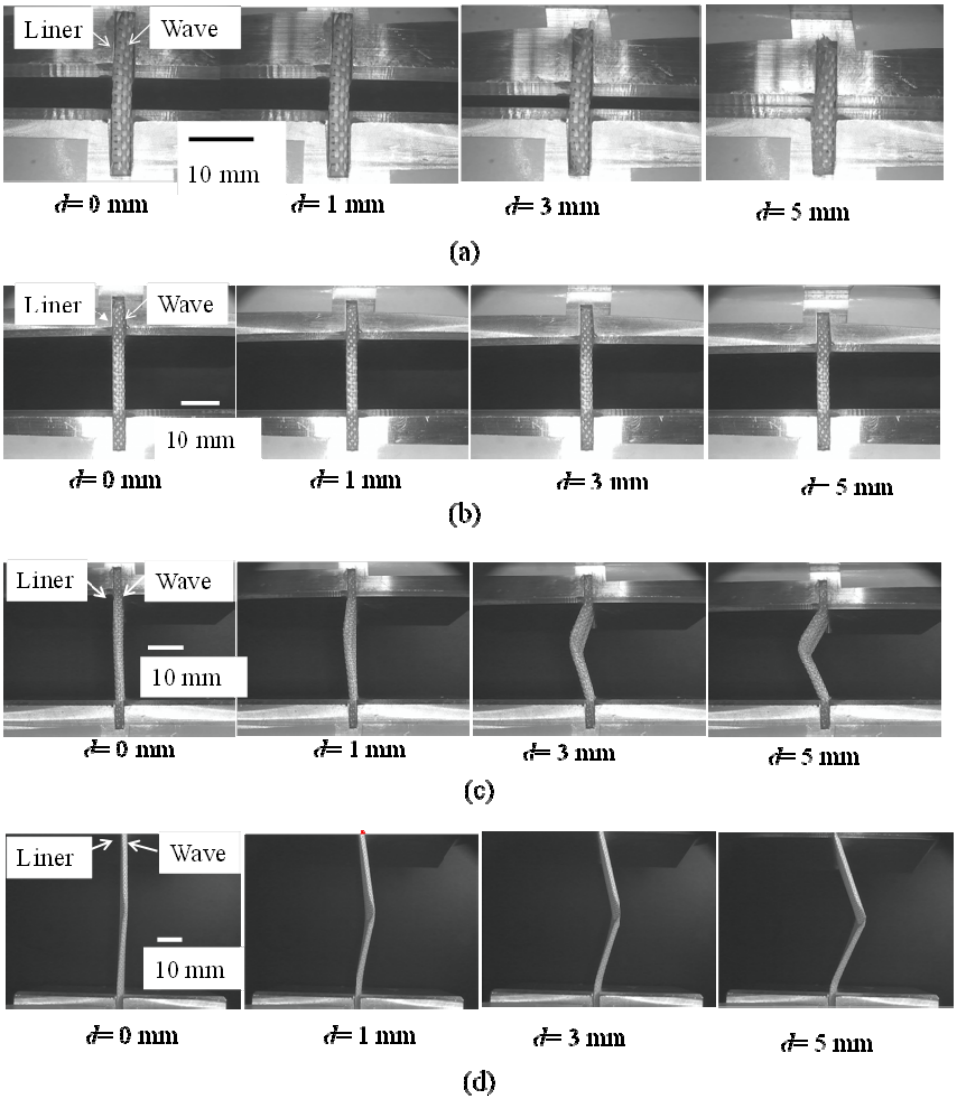

Figure 8. Deformation behavior of GFSS during in-plane compression at a width of groove w_{gs} = 3mm without dipping instant adhesives (not reinforced). (a) In a case of the height of free zone h_f = 5 mm; (b) In a case of the height of free zone h_f = 20 mm; (c) In a case of the height of free zone h_f = 40 mm; (d) In a case of the height of free zone h_f = 80 mm.

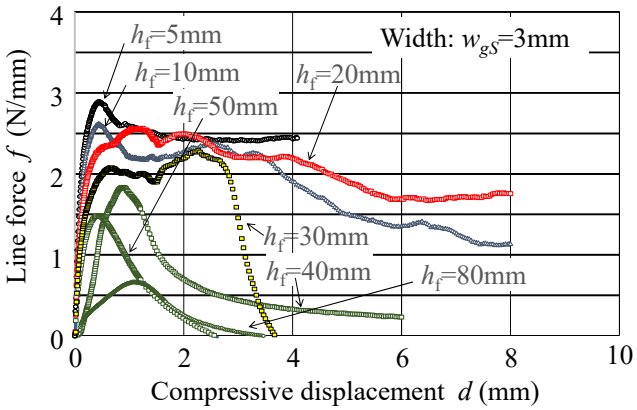

Figure 9. Load response diagram of compressive test of straight panel when varying h_f without dipping instant adhesives (not reinforced).

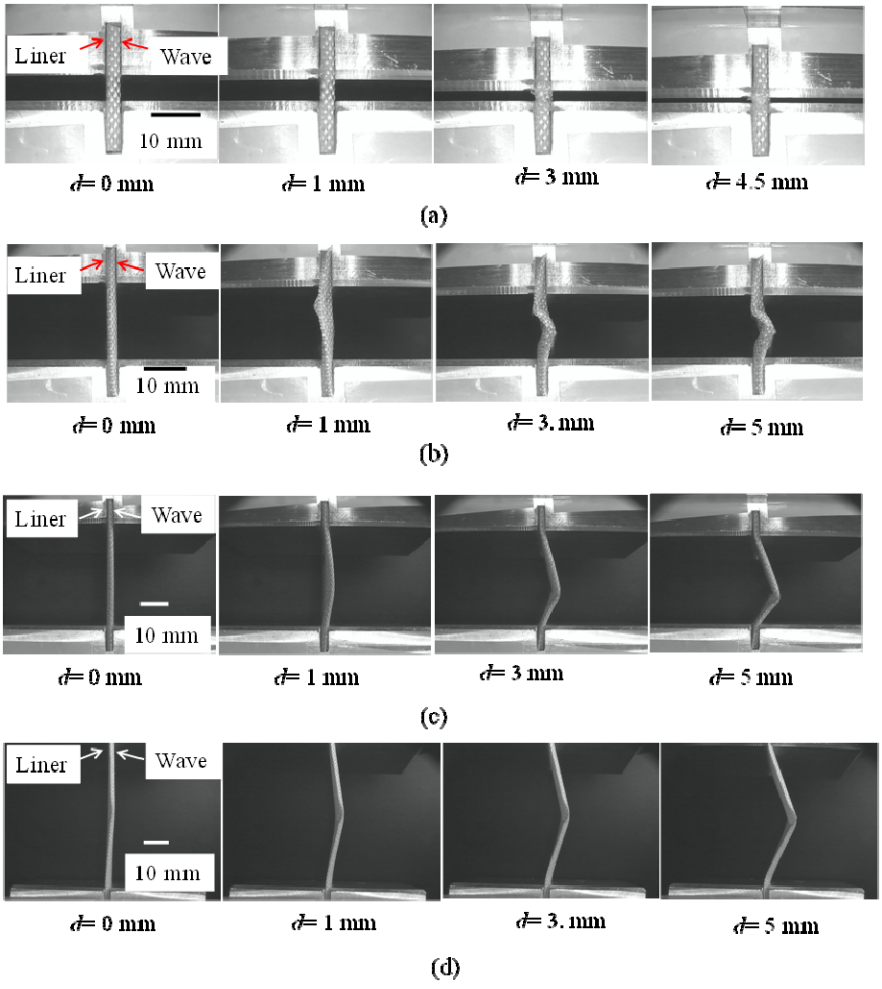

Figure 10. Deformation behavior of GFSS during in-plane compression at a width of groove w_{gs} = 3mm with dipping instant adhesives (reinforced by glue). (a) In a case of the height of free zone h_f = 5 mm; (b) In a case of the height of free zone h_f = 20 mm; (c) In a case of the height of free zone h_f = 40 mm; (d) In a case of the height of free zone h_f = 80 mm.

Figure 11 shows the relationship between the compressive line force f and the displacement of the upper edge holder d, when the both ends of the panel was dipped with instant adhesives.

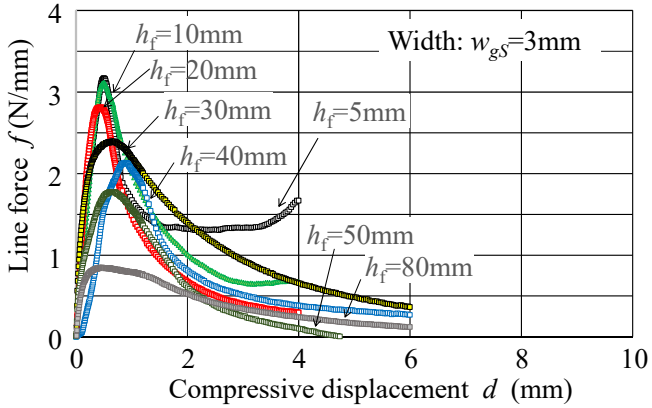

Figure 11. Load response of compressive test of straight panel when varying h_f with dipping instant adhesives (reinforced by glue).

In this experiment, the peak maximum of line force remarkably occurred in the early stage (d < 2 mm). When h_f = 5 mm, as any out-of-plane buckling was not observed, a certain level of compressive resistance was kept for a range of d < 4 mm. The out-of-plane buckling occurred for h_f >10 mm. This transition condition seemed to be caused from the crtical condition of ECT: $4h_0$ = 12 mm. Seeing Figures 8–11, it was found that a certain saturated resistance of the line force appreaed for h_f < 30 mm when the lateral buckling did not occur at that timing. Since this saturation apted to disappeare or vary when the compressive displacement increased furthermore, that was here called as the quasi-saturated. This seemed to be caused from the edge crush mode of the panel.

Figure 12 shows the quasi-saturated resitance of line force after passing the peak maximum. Here, to briefly detect the saturated state of the compressive resistance, the quaqsi-saturated line force was evaluated for a short duration when d > 3mm. The quasi-saturated state was detected for h_f <30 mm in Figure 12. In Figure 9, the short height condition of h_f < 30mm showed a certain resistance larger than 2 N/mm due to this quasi-saturated state by the in-plane end crushing mode, while the long height condition of h_f > 30mm showed a large lateral deflection characterized by the triangle-like deflection. In the latter, only one peak force occurred, whereas there were some quasi-saturated resistance by the in-plane end-crushing mode or the out-of-plane bulging of the panel in the former case. In the middle zone of 20 mm < h_f < 30 mm, the deformation consisted of the in-plain end crush mode and the lateral defelection mode under the end-fixing condition, although the former (in-plane end-crush) was the primary mode when the both ends pressure fitted to the groove's bottoms by the initial crushing of the both ends (it was performed without instant adhesives). In the case of the reinforced condition shown in Figure 11, the reinforced ends contributed to make the span length of the panel larger and then the lateral deflection as a pillow's buckling appeared to be easily generated. Hence, the case of h_f < 20 mm was recognized as the in-plane end-crush mode, while the case of h_f > 20 mm behaved as the lateral deflection mode when considering the dipping of instant adhesives.

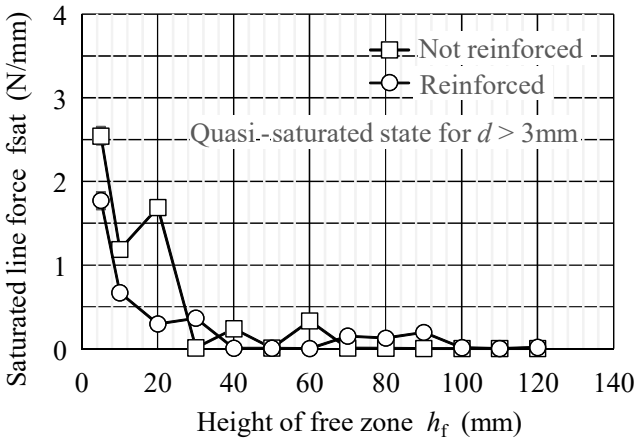

Figure 12. Quashi-saturated line force derived from Figures 9 and 11.

Figure 13 shows the relationship between the peak maximum line force f_p and the height of free zone h_f. Since there were sometimes multiple peaks of the line force in a range of compressive displacement 8 mm when the instant adhesives were not dipped on the both ends, the first peak was additionally picked up when the peak maximum was detected after the first peak occurrence. In Figure 9, the case of $h_f = 30$ mm was a representative response which included several peaks. Herein, the lateral deflection was not detected at the first peak position ($d < 1$ mm) but that was a little observed at the secondary peak position ($d \approx 2$ mm) when $h_f = 30$ mm.

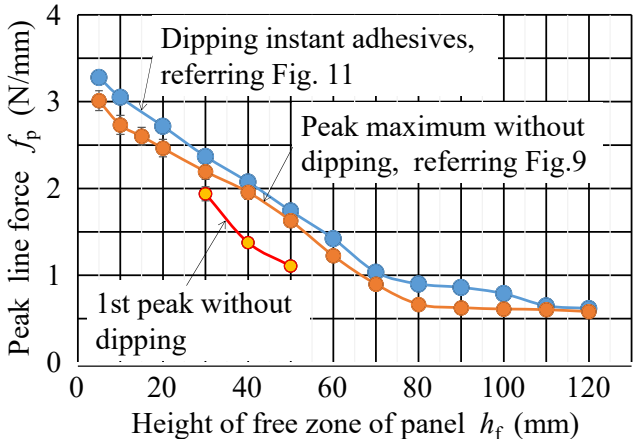

Figure 13. Dependency of peak maximum line force on height of free zone when $w_{gS} = 3$ mm.

Seeing Figure 13, the peak maximum of reinforced case was about 0.2–0.3 N/mm larger than that of non-reinforced case. This difference seemed to be caused from the crushing resistance of the both ends due to the dipping reinforcement of instant adhesives.

For the range of $h_f < 80$ mm, as the peak maximum line force f_p linearly decreased with h_f, the following approximations Eqs 3 and 4 were derived by the least square method. Here, The values of R^2 were the coefficient of determination with Eqs 3 and 4, respectively.

$$f_p = -0.0307\, h_f + 3.10 \text{ (non-reinforced for } 5 < h_f < 80 \text{ mm, } R^2 = 99.6\%) \quad (3)$$

$$f_p = -0.0323\ h_f + 3.375 \text{ (reinforced for } 5 < h_f < 80 \text{ mm, } R^2 = 99.6\%) \quad (4)$$

Figure 14 shows the critical buckling strength of the panel using the pillar's buckling theory Eq 2 and the values of bending stifness D of Table 2. The approximations of Eqs 3 and 4 were also plotted in this graph.

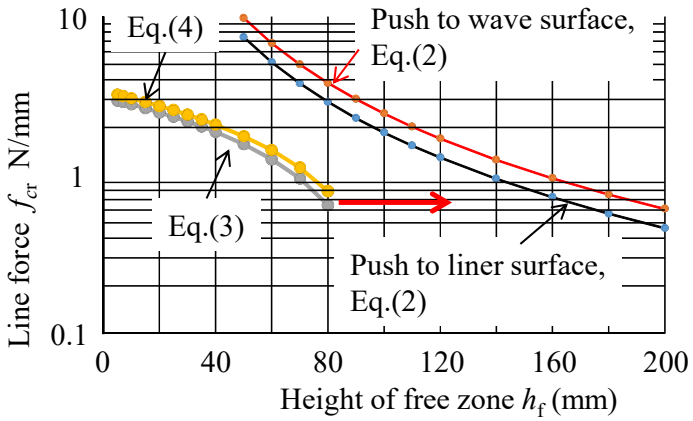

Figure 14. Calculated strength of Eulerian equation Eq 2 and experimental approximations.

Seeing Figure 14, as the gradient $\partial f_p/\partial h_f$ of Eqs 3 and 4 was almost equal to the results of Eq 2 for h_f = 40–80 mm, the buckling behavior in this range appeared to be explained from the Eulerian equation of Eq 2, except for the absolute value of buckling strength. Its mismatching ratio was estimated as 4 times for h_f = 40–80 mm. For the range of h_f < 30 mm, the buckling behavior was understood as the edge crush mode (in-plane crushing or buldging of the panel without a lateral deflection). When increasing the height of the panel for h_f = 80–120 mm, the decreasing of compressive strength f_p was quite slow, or almost constant. Seeing Figure 8d and Figure 10d at d = 1 mm, the initial buckling seemed to be caused as a triangle bending of the panel at the clamped-end position of upper/lower grooves. This saturation of f_p seems to be caused from the complexed mode such as a cylindrical-shell buckling [19] for h_f = 80–120 mm, because the buckling strength was almost independent to the height of the panel.

3.3. Buckling directions of panel

The direction of lateral deflection of the panel is classified in two modes: (a) it moves from the liner to the wave side as shown in Figure 3(b-1), or (b) it moves from the wave to the liner side as Figure 3(b-2). From the results of three point bending test of GFSS and Table 2, since the bending stiffness of pushing the wave surface was 32% stronger than that of pushing the liner surface, the lateral deflection of the in-plane compressive test seemed to be eccentricly the pattern of Figure 3(b-1) direction. However, the results included two patterns of Figure 3(b-1) and (b-2). Figure 15 shows the occurrence distribution of buckling directions (Red: the deflection moved to the liner side or Blue: it moved to the wave side at the center zone of the panel). Seeing the experimental results, it was found that the initialization appeared to be affected by the reinforcement by the instant adhesives, while the pattern of Figure 3(b-2) (move to liner) apted to easily occur for h_f > 60 mm. Considering the difference of bending stiffness with two buckling directions and the triangle buckling of the panel at

the early stage ($d \approx 1$ mm), the initiation of the first buckling seemed to occur at the clamped-end position of the groove. Namely, if the pattern of Figure 3(b-1) occurs at the clamped-end position of the groove, then the central zone tends to move to the opposite side, to the liner side. On the other hand, if the pattern of Figure 3(b-1) occurs at the central zone, the mode was not changed. Hence, two patterns of buckling direction are possible, principally.

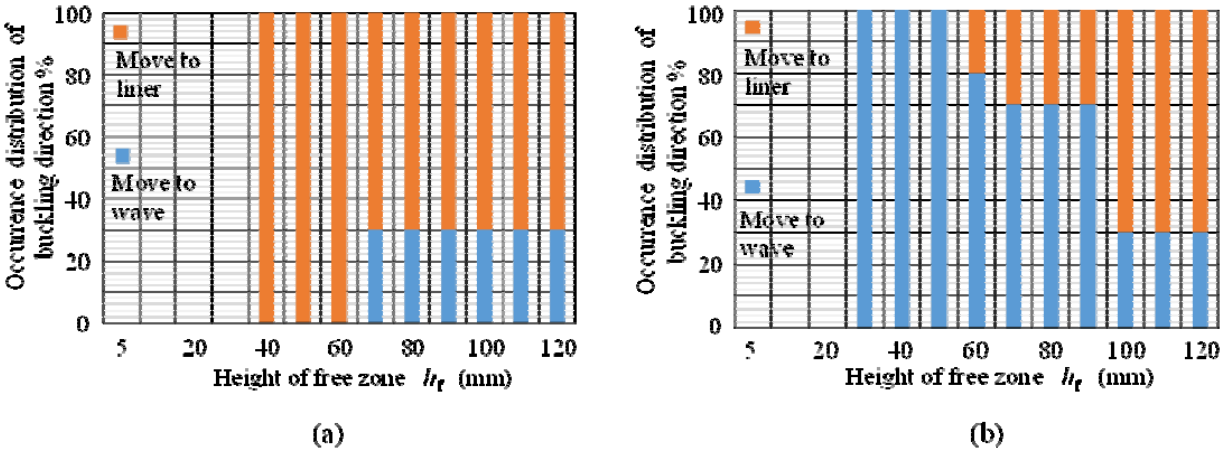

Figure 15. Occurrence distribution of buckling direction. (a) Not reinforced (without dipping instant adhesives); (b) Reinforced (dipping instant adhesives).

3.4. Effects of groove's width on the buckling strength

Since the freedom of rotation at the clamped-end position of the holder's groove seems to be important to determine the critical buckling strength of the panel, the width of the holder's groove w_{gS} was varied from 3.0 mm up to 4.0 mm when the both ends of the panel was not reinforced by the instant adhesives.

Figure16 shows representative compression processes of the straight panel which had $h_f = 5$, 20, 40, 80 mm and $w_{gs} = 4$mm without dipping instant adhesives on the both ends. Figure 17 shows the relationship between the compressive line force f and the displacement of the upper edge holder d. when choosing $w_{gS} = 4$ mm and $h_f = 10$ mm without dipping instant adhesives on the both ends.

Seeing Figure 16, the upper ends (and the lower ends) of the panel were crushed and clearly inclined in one side (left or right) at the groove zone, due to a 1mm-clearance between the groove's width and the panel's thickness. This inclination of the ends of the panel in the groove zone seems to cause some decreasing of the gradient $\partial f / \partial d$ at the early stage ($0 < d < 0.5$ mm). As the result, the peak maximum line force f_p decreased with w_{gS}, while the corresponded displacement d_p apted to increase.

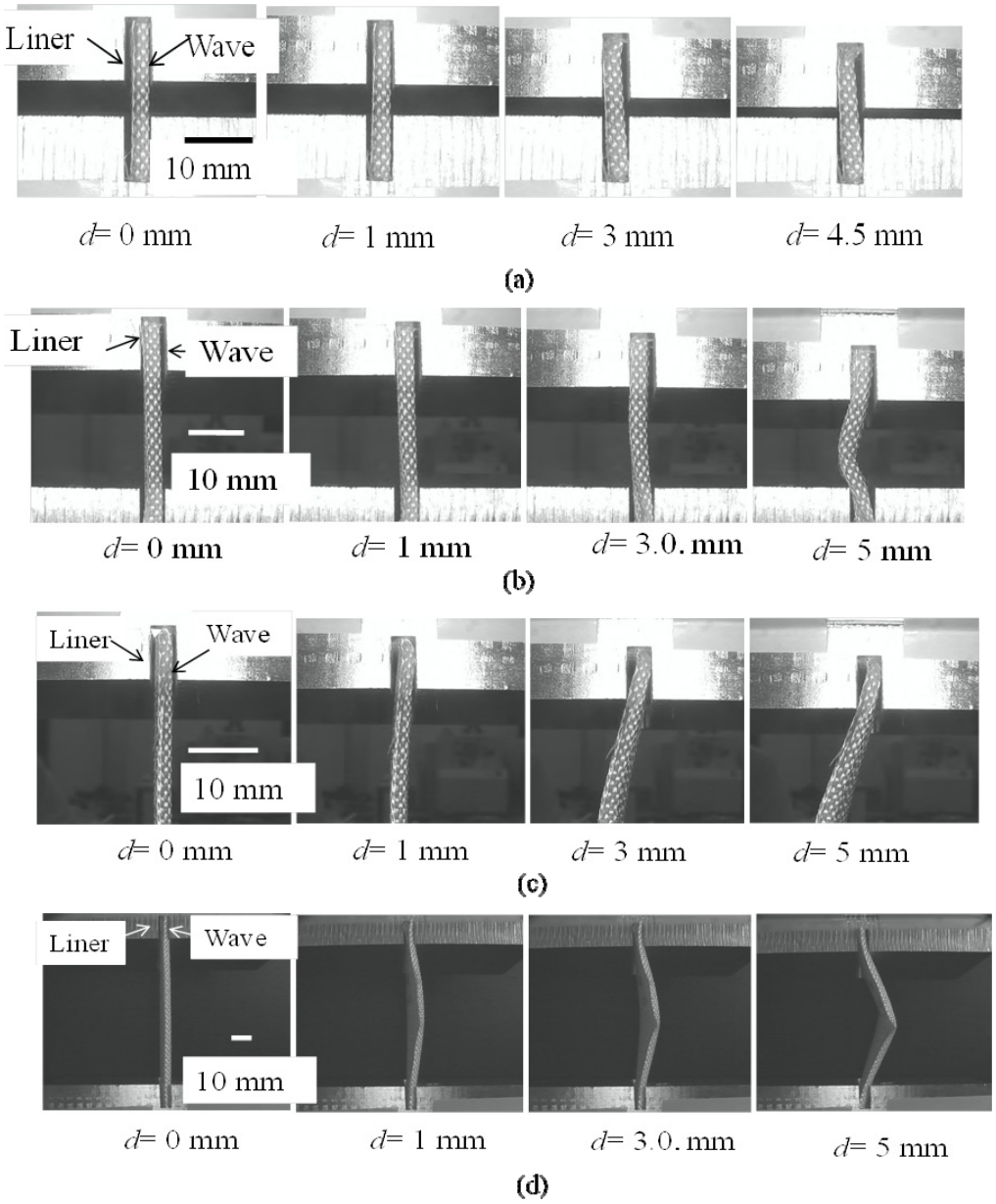

Figure 16. Deformation behavior of GFSS during in-plane compression at a width of groove w_{gs}= 4 mm without dipping instant adhesives (not reinforced). (a) In a case of the height of free zone h_f =5 mm, (b) In a case of the height of free zone h_f =20 mm, (c) In a case of the height of free zone h_f =40 mm, (d) In a case of the height of free zone h_f =80 mm.

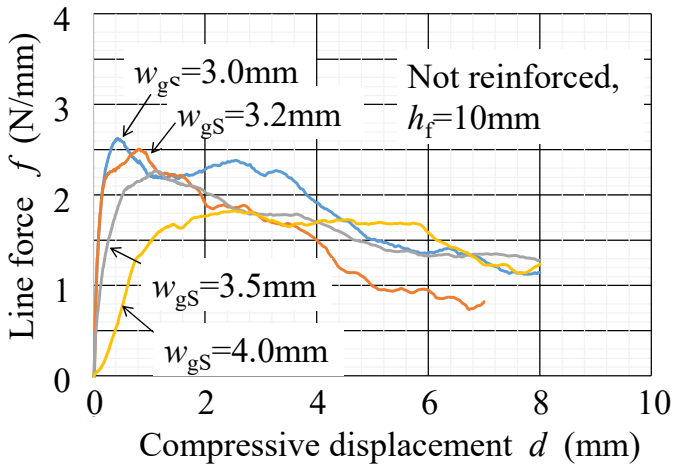

Figure 17. Load response diagram of compressive test of straight panel at h_f = 10 mm under varying groove's width w_{gS} without dipping instant adhesives (not reinforced).

Figure 18 shows the peak maximum line force for h_f = 5–80 mm. When h_f < 50 mm (=16.7h_0), f_p decreased with w_{gS}. Since this relationship between f_p and w_{gS} was similar for h_f < 50 mm, focusing on the case of h_f = 40 mm, a linear approximation of f_p with w_{gS} was derived from Figure 18, and its relation was shown as Eq 5. Herein, the dependency of f_p on w_{gS} disappeared for h_f > 70 mm.

$$f_p = 4.725 - 0.916\, w_{gS} \quad (\text{for } w_{gS} = 3\text{–}4 \text{ mm at } h_f = 40 \text{ mm}, R^2 = 98.9\%) \tag{5}$$

Seeing the first peak without dipping in Figure 13, it disappeared for h_f > 60 mm. The dependency of f_p in Figure 18 also disappeared for h_f > 60 mm. Therefore, the buckling strength of the panel seems to be primarily determined by the height of panel h_f, not by the local crushing condition of both ends of the panel in the holder's groove, when h_f > 60 mm.

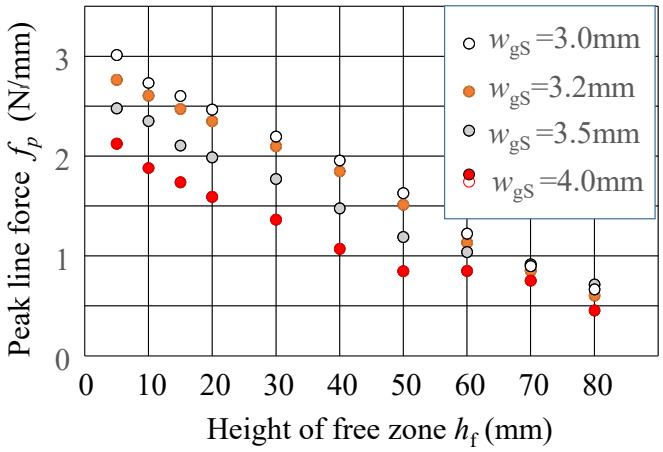

Figure 18. Dependency of peak maximum line force on width of holder's groove when both ends were not reinforced by instant adhesives.

4. Conclusions

To perform an in-plane compressive test of fragile glass fibre based single faced corrugated structure sheet (GFSS), and to reveal the buckling strengh of the straight panel of GFSS, a holding tool which has appropriate groove for supporting the panel in the perpendicular attitude was developed. To discuss the buckling strength under an in-plane-compressive loading of GFSS across the machine producing direction (along the flute's longitudinal direction), a three-point-bending flextural test of GFSS was preliminary carried out and a reinforced condition of the both ends of the panel was inspected by dipping a small volume of instant adhesives. Furthermore, to investigate the effects of clearance of the groove, several width of the groove were prepared for the experiment.

The revealed results were as follows:

(1) A plain panel of GFSS without dipping instant adhesives was locally crushed at the both ends of the panel in the holder's groove, while the panel reinforced by dipping the instant adhesives (liquid arone alpha) on the both ends stably resisted in the holder's groove and it had the higher strength of 0.2–0.3 N/mm when varying the height of free zone h_f = 0.5–120 mm.

(2) Using the three-point-bending stiffness and the Eulerian piller's theory Eq 2, the critical buckling strength of the panel was estimated. The gradient of the buckling strength $\partial f_p/\partial h_f$ with h_f matched to the theoretical behavior for a certain range 40mm < h_f < 80mm.

(3) When h_f < 30 mm, the compressive deformation of the panel behaved as an end-crush and in-plane bulging without any lateral deflection. The transition condition was almost estimated as 4–10 times of the height (h_0 = 3 mm) of GFSS.

(4) When choosing 120 mm > h_f > 80 mm, the decreasing tendency of f_p was changed (quite slow state), compared to the middle range 40 mm <h_f < 80 mm.

(5) A local initiation of buckling was revealed at the clamping-end position of the holder's groove, and the lateral deflection profile of the panel behaved as a triangle-like folding of the panel when h_f > 40 mm.

(6) The dependency of f_p on the holder's width w_{gS} almost disappeared for h_f > 60mm.

Acknowledgments

The authors thank Syotaro Takeda of KUBO corporation, for his assistance with preliminary experiments and preparing glass fiber based fabrics structural sheets.

Conflict of interest

All authors declare there is no conflict in this paper.

References

1. Kubo corporation, Glass fibre based structural sheet, 2017. Available from: http://www.kubo-co.net/.
2. Kirwan MJ (2013) Corrugated fiberboard packaging, *Handbook of Paper and Paperboard Packaging Technology*, 2 Eds., John Wiley & Sons, 313–321.

3. Jonson G (1999) *Corrugated Board Packaging*, 2 Eds., Leather head*:* Pira International, 145–159.
4. Lubin G (1982) Characterization of corrugated board, *Handbook of Composite*, Springer, Boston, MA, 145–149.
5. Mark RE, Habeger C, Borch J, et al. (2002) Characterization of corrugated board, *Handbook of Physical Testing of Paper*, 2 Eds., CRC Press, 1: 571–574.
6. Twede D, Selke SM, Kamdem D, et al. (2015) Single face, *Cartons, Crafts and Corrugated Board: Handbook of Paper and Wood Packaging Technology*, DEStech publication, 460–464.
7. Twede D, Selke SEM, Kamdem D, et al. (2015) *Cartons*, *Crafts and Corrugated Board: Handbook of Paper and Wood Packaging Technology*, DEStech publication, 250–252.
8. Bronkhorst CA, Keith AB (2002) Deformation and failure behaviour of paper (Edge wise crush test), In: Mark RE, Habeger C, Borch J, et al., *Handbook of Physical Testing of Paper*, 2 Eds., CRC Press, 1: 401–409.
9. Nagasawa S, Kudo H, Songtam L, et al. (2017) Tensile characteristics of glass fiber based single face board. *Procedia Eng* 207: 78–83.
10. Laosuwan S, Nagasawa S, Umemoto K (2020) Development of tensile fixture with corrugated structure sheet and estimation of tensile strength of glass fibre fabrics based single face corrugated structure sheet. *AIMS Mater Sci* 7: 75–92.
11. Matsushima S, Okuda T, Miyauchi O, et al. (1982) Strength of tensile deformation for corrugated fibre board. *Japan TAPPI J* 36: 377–387.
12. Wahab N, Arafah A, Fukuzawa Y et al. (2016) Estimation of corrugated cardboard strength using tensile test, In: MFB Abdollah, MAB Salim, TB Tuan, *Proceeding of Mechanical Engineering Research Day 2016*, Melaka: Centre for Advanced Research on Energy.
13. Cox HL (1952) The elasticity and strength of paper and other fibrous materials. *Br J Appl Phys* 3: 72–79.
14. T glass, Niitobo corporation, 2019. Available from: https://www.nittobo.co.jp/business/glassfibre/sp_material/t-glass.htm.
15. Loewenstein KL (1973) *The Manufacturing Technology of Continuous Glass Fibres*, 2–94, Elsevier Scientific.
16. Loewenstein KL (1975) The manufacture of continuous glass fibres. *Platinum Met Rev* 19: 84–87
17. Popil RE (2017) Bending stiffness of corrugated board, *Physical Testing of Paper*, UK: Smithers Pira, 67–77.
18. Timoshenko S (1955) Elementary theory and problems, Strength of materials, 3 Eds., D. Van Nostrand Company, 252–266.
19. Mihara Y, Kobayashi T, Fujii F (2011) Postbuckling analyses of elastic cylinderical shells under axial compression. *Trans JSME* 77: 582–589.